

Role of surface charge in determining the biological effects of CdSe/ZnS quantum dots

Qiangqiang Liu^{1,*}Hongxia Li^{1,*}Qiyue Xia¹Ying Liu¹Kai Xiao^{1,2}

¹National Chengdu Center for Safety Evaluation of Drugs, State Key Laboratory of Biotherapy, Collaborative Innovation Center for Biotherapy, West China Hospital, ²Laboratory of Non-Human Primate Disease Model Research, State Key Laboratory of Biotherapy, Collaborative Innovation Center for Biotherapy, West China Hospital, Sichuan University, Chengdu, People's Republic of China

*These authors contributed equally to this work

Abstract: The growing potential of quantum dots (QDs) in biomedical applications has provoked the urgent need to thoroughly address their interaction with biological systems. However, only limited studies have been performed to explore the effects of surface charge on the biological behaviors of QDs. In the present study, three commercially available QDs with different surface coatings were used to systematically evaluate the effects of surface charge on the cellular uptake, cytotoxicity, and in vivo biodistribution of QDs. Our results demonstrated that charged QDs entered both cancer cells and macrophages more efficiently than neutral ones, while negative QDs internalized mostly. Upon entry into cells, QDs were localized in different subcellular compartments (eg, cytoplasm and lysosomes) depending on the surface charge. Interestingly, inconsistent with the result of internalization, positive QDs but not negative QDs exhibited severe cytotoxicity, which was likely due to their disruption of cell membrane integrity, and production of reactive oxygen species. Biodistribution studies demonstrated that negative and neutral QDs preferentially distributed in the liver and the spleen, whereas positive QDs mainly deposited in the kidney with obvious uptake in the brain. In general, surface charge plays crucial roles in determining the biological interactions of QDs.

Keywords: cellular uptake, uptake pathways, intracellular distribution, reactive oxygen species, cytotoxicity, biodistribution

Introduction

Quantum dots (QDs) are nanometer-sized inorganic nanomaterials with exceptional optical and electronic properties, which exhibit distinct advantages over traditional fluorescent organic dyes in terms of great signal brightness, high-quantum yield, rock-solid photo-stability, tunable broad excitation, and narrow emission spectra.^{1,2} QDs have shown great promise in the biomedical applications, including labeling of cellular proteins, sensitive cellular imaging, real-time tracking, fluorescence resonance energy transfer sensors, visible drug carriers, in vivo animal imaging, and cancer theranostics.³⁻⁶ For instance, fluorescent QDs can be conjugated with bioactive moieties (eg, antibodies, peptide, aptamers, and small-molecule ligand) to target specific biologic events and cellular structures, such as labeling neoplastic cells, cell membrane receptors, DNA, and peroxisomes.⁷⁻¹⁰

The increasingly widespread use of QDs in biomedical applications raises concerns about the potential risk of human exposure, interactions with biological systems, and toxicological implications. Nanomaterials with particular physicochemical properties may potentially enter tissues, cells, and organelles, and interact with functional biomolecular structures to induce toxicity.^{11,12} Previous reports regarding the toxicity of QDs have presented conflicting results. Several papers indicated that certain QDs were cytotoxic, whereas several other in vitro and in vivo studies did not observe QD-induced cytotoxicity.¹³⁻¹⁵ The discrepancies in the current literature regarding

Correspondence: Kai Xiao
National Chengdu Center for Safety Evaluation of Drugs, State Key Laboratory of Biotherapy, Collaborative Innovation Center for Biotherapy, West China Hospital, Sichuan University, 28 Gaopeng Avenue, High Technological Development Zone, Chengdu 610041, Sichuan, People's Republic of China
Tel +86 28 8332 6313
Fax +86 28 8517 3043
Email iamxiaokai@hotmail.com

QD toxicity may be attributed to several factors, including individual differences of physicochemical properties, lack of toxicology-based studies, and a variety of dosage/exposure concentrations.^{16,17}

It is noted that not all QDs are alike, and each individual type of QDs may have its unique physicochemical properties (eg, composition, size, surface charge, and functionalization), which in turn determines its biological responses.^{18–23} For example, particle size was shown to be a determining factor in subcellular distribution and cytotoxicity. Lovrić et al reported that smaller (2.2 nm) cationic cadmium telluride (CdTe) QDs were localized in the nuclear compartment, while larger (5.2 nm) cationic QDs were observed to localize throughout the cytosol; and smaller QDs exhibited more pronounced cytotoxicity than larger QDs at equal concentrations.²¹ Surface charge has been also considered as an important determinant of biological effects of nanoparticles, including cellular uptake, permeability of physiological barrier, toxicity, absorption, distribution, metabolism, and excretion. However, the specific role of surface charge in different type of nanoparticle systems could be different. For example, Juliano and Stamp reported that negatively charged liposomes were eliminated more rapidly than neutral and positively charged ones, which was explained by the tendency of negatively charged liposomes to coalesce in the presence of proteins and calcium ion in blood plasma.²⁴ Conversely, Xiao et al demonstrated that micelles with high surface charge, either positive or negative, tended to be cleaned up by macrophages, resulting in undesirable high liver uptake; whereas the liver uptake was much lower when the surface charge of micelles was neutral or slightly negative.²⁵ For QDs, the studies focusing on the surface charge effects are very limited, and only a few *in vitro* studies demonstrated that surface charge might be involved in the endothelium crossing and cellular uptake of QDs.^{26,27} However, the mechanisms underlying the distinct cellular interactions of various QDs have not been fully addressed. In addition, there has been relatively scant information regarding the effect of surface charge on *in vivo* behavior of QDs.

In the present study, we comprehensively investigated the roles of surface charge in determining the cellular uptake, *in vitro* cytotoxicity, and *in vivo* biodistribution of QDs. Commercially available CdSe/ZnS QDs with different surface coatings, including polydiallyldimethylammonium chloride (PDDA, positive charge), carboxylic acid (CA, negative charge), and polyethylene glycol (PEG, neutral), were employed in this study. The precise control in the physicochemical properties of QDs allowed us to evaluate the biological effects of surface charge of QDs under the identical

other conditions (eg, the same composition and similar particle sizes). The uptake efficiencies, pathways, and intracellular fates of different charged QDs were examined in MDA-MB-231 breast cancer cells and RAW 264.7 macrophages. The *in vitro* cytotoxicities of QDs against different cell lines, and the underlying mechanisms were further explored. Finally, the blood clearance, biodistribution, and *in vivo* toxicity of different charged QDs were investigated in BALB/c mice after intravenous administration. Our study provides invaluable information in designing tailored nanomedicines for diagnostic, imaging, and drug delivery purposes.

Materials and methods

Materials

CdSe/ZnS QDs coated with positive PDDA (PDDA-QDs, Catalog number QSQ-580), CdSe/ZnS QDs coated with negative CA (CA-QDs, Catalog No QSH-580), and CdSe/ZnS QDs coated with neutral PEG (PEG-QDs, Catalog number QMG-580) were purchased from Ocean Nanotech, LLC (San Diego, CA, USA). Hoechst 33342, LysoTracker Green, and DiOC6(3) were purchased from Thermo Fisher Scientific, Waltham, MA, USA. CellTiter 96[®] Aqueous Non-Radioactive Cell Proliferation Assay Kit and CytoTox 96[®] Non-Radioactive Cytotoxicity Assay Kit were purchased from Promega Corporation (Fitchburg, WI, USA). Fluorescein isothiocyanate (FITC) Annexin V Apoptosis Detection Kit was purchased from BD Biosciences. 2',7'-Dichlorofluorescein diacetate (DCF-DA), endocytosis inhibitors, including chlorpromazine (CPZ) hydrochloride, amiloride hydrochloride hydrate, filipin III and all other chemicals were purchased from Sigma-Aldrich (St Louis, MO, USA).

Characterization of QDs

The morphology and particle size of QDs were observed on a Philips CM-120 transmission electron microscope (TEM) (Philips, Eindhoven, Netherlands) operating at an acceleration voltage of 80 kV. QDs were homogeneously dispersed in water, and one drop of the suspension was deposited on a TEM grid, dried, and evacuated before analysis.

The stability in particle size of QDs in fetal bovine serum (FBS) was measured by dynamic light scattering (DLS) and TEM, respectively. QDs with various surface coatings were incubated with 50% FBS for different time periods. The size distribution of QDs in the presence of FBS was measured by DLS (Malvern Instruments, Malvern, UK). The sample was also dropped onto a TEM grid, and the morphology of QDs was observed under a Hitachi TEM system (Hitachi High-Technologies, Ibaraki, Japan).

Cell culture

This study was approved by the local ethic committee of West China Hospital, Sichuan University, and cell lines were purchased from ATCC. MDA-MB-231 cells, RAW 264.7 cells, and BT-20 cells were, respectively, cultured in IL-15, Dulbecco's Modified Eagle's Medium and McCoy's 5A Medium supplemented with 10% FBS, 100 U/mL penicillin G, and 100 mg/mL streptomycin at 37°C using a humidified 5% CO₂ incubator.

Cellular uptake of different charged QDs

MDA-MB-231 cells (1×10^4) were seeded in 8-well chamber tissue culture slides. When the cells became almost 80% confluent, cells were treated with 40 nM QDs with various surface charges, then incubated in 5% CO₂ incubator at 37°C for 30 minutes, 1, 2, and 4 hours, respectively. The nuclei were counterstained by Hoechst 33342. Live cells imaging was observed by confocal fluorescence microscopy (Carl Zeiss Meditec AG, Jena, Germany).

Uptake pathways of different charged QDs

The effect of temperature block was studied by preincubating the MDA-MB-231 cells at 4°C for 1 hour and treatment with different charged QDs for 2 hours at 4°C. To study the effects of different endocytosis inhibitors on the cellular uptake of QDs, MDA-MB-231 cells were preincubated for 1 hour at 37°C with the following inhibitors at concentrations that were not toxic to the cells: filipin III (1 mg/mL) to inhibit caveolae formation, amiloride (50 mM) to inhibit macropinocytosis, or CPZ (10 mg/mL) to inhibit the formation of clathrin vesicles. Following the preincubation, 40 nM QDs with different surface charges were added into the medium containing the inhibitors, and the cells were incubated at 37°C for 2 hours. The cells were washed three times with ice-cold phosphate buffered saline (PBS), fixed with fresh 4% paraformaldehyde for 10 minutes at room temperature, and the nuclei were stained with 4',6-diamidino-2-phenylindole. The cells were observed under confocal fluorescence microscopy (Carl Zeiss Meditec AG).

In addition, the effects of temperature and endocytosis inhibitors on the cellular uptake of QDs were quantitatively analyzed by flow cytometry. Briefly, MDA-MB-231 cells (1×10^5) were seeded in 6-well cell culture plate. When the cells became almost 80% confluent, cells were harvested into different vials to preincubated at 4°C or endocytosis inhibitors for 1 hour. Following the preincubation, QDs with different surface charges (final concentration of 40 nM) were added into the medium that containing the inhibitors and the cells were incubated at 37°C (or 4°C for the low temperature

group) for 2 hours. Then, the cells were washed three times with PBS, and subjected to flow cytometric analysis, with the excitation wavelength of 488 nm and the emission wavelength of 580 nm. Approximately 1×10^4 counts were collected for each sample.

Intracellular location of QDs in live cells

MDA-MB-231 cells and RAW 264.7 macrophages (1×10^4) were seeded in the 8-well chamber slides. After reaching 80% confluence, the cells were treated with different charged QDs (40 nM). After 2-hour incubation, LysoTracker Green (75 nM) or DiOC6(3) (40 nM) was added in the medium, and the cells were incubated for another 30 minutes, then incubated with Hoechst 33342 for 10 minutes to label the cell nuclei. The cells were rapidly washed with ice-cold PBS and replaced with fresh medium, and then the live cells were observed under the confocal fluorescence microscopy (Carl Zeiss Meditec AG).

Transmission electron microscopy

MDA-MB-231 cells (1×10^4) were seeded in the 8-well chamber Permaxox® slides and cultivated until 80% confluence. Cells were incubated for 2 hours with different charged QDs (40 nM). Then, the cells were washed and fixed with 2.5% glutaraldehyde in cacodylate buffer (pH 7.2). The samples were postfixed with osmium tetroxide, dehydrated in sequential ethanol solutions, embedded in resin, and finally ultramicrotomed. TEM images were obtained at 80 kV on a Philips CM-120 TEM.

In vitro cytotoxicity and lactate dehydrogenase release

MDA-MB-231 cells, BT-20 cells, and RAW 264.7 macrophages (1×10^4) were seeded in 96-well plates, and exposed for 24 hours with different charged QDs at concentrations ranging from 0 to 40 nM, respectively. After 24-hour incubation with QDs, the cell viability was measured by MTS assay.

MDA-MB-231 cells (5×10^3) were seeded in 96-well plates and cultivated until 80% confluence, then treated with various QDs at concentrations up to 80 nM. At 24 hours, the supernatant was collected in a 96-well plate to analyze the lactate dehydrogenase (LDH) release by using the CytoTox 96® Non-Radioactive Cytotoxicity Assay.

Hemolysis test

The suspension of erythrocytes in PBS at 2% was prepared by using freshly harvested mouse blood. Then, 200 µL aliquot of the erythrocytes suspension was mixed with various concentrations of QDs (ranging from 2.5 to 320 nM). Deionized

water and PBS solution were used as positive control and negative control, respectively. After 4 hours of incubation at 37°C, the mixtures were centrifuged at 3000 rpm for 5 minutes, and 100 µL of supernatant of all samples were transferred to a 96-well plate. Free hemoglobin in the supernatant was measured by the absorbance at 540 nm using a microplate reader (SpectraMax M2, Molecular Devices LLC, Sunnyvale, CA, USA). The percent hemolysis of red blood cells was calculated using the following formula:

$$\text{RBCs hemolysis} = \frac{OD_{\text{sample}} - OD_{\text{negative control}}}{OD_{\text{positive control}} - OD_{\text{negative control}}} \times 100\%. \quad (1)$$

Reactive oxygen species

MDA-MB-231 cells (1×10^4) were seeded in 8-well chamber Permanox® slides. After reaching 80% confluence, cells were incubated with various concentrations of QDs (from 10 to 80 nM) for 2 hours. Intracellular reactive oxygen species (ROS) was measured using 10 µM DCF-DA. ROS production was qualitatively observed by confocal fluorescence microscope, and the green fluorescence intensity indicated the level of ROS production. For quantitative analysis, the fluorescence intensities of the cells were measured by flow cytometry, and approximately 1×10^4 counts were collected for each sample.

Mitochondrial membrane potential

MDA-MB-231 cells (1×10^4) were seeded in 8-well chamber Permanox® slides. After reaching 80% confluence, cells were incubated with various concentrations of QDs (10, 20, and 40 nM) for 2 hours. After the cells were washed three times with PBS, they were treated with 40 nM of DiOC6(3) for 30 minutes and subjected to fluorescence microscopy imaging.

Apoptosis and cell cycle analysis

MDA-MB-231 cells (5×10^5) were seeded onto 6-well plate and incubated for 24 hours in culture medium containing different concentrations of QDs (0.4 and 2 nM). After incubation, cells were washed three times with PBS, trypsinized, and resuspended in PBS. Cells were stained for 30 minutes with Annexin V-FITC and propidium iodide (PI), and then analyzed by flow cytometry. For the cell cycle analysis, cells were fixed in cold 70% ethanol after 24-hour treatment as mentioned earlier. Then, cells were washed with PBS, treated with ribonuclease, and stained with PI (10 µg/mL), followed by flow cytometric analysis. Approximately 1×10^4 counts were collected for each sample.

In vivo toxicity, blood clearance, and tissue biodistribution

Male BALB/c mice (22–25 g) were purchased from the breeding center of Guangdong Medical Laboratory Animal, People's Republic of China. All animals were kept under pathogen-free conditions according to the Association for Assessment and Accreditation of Laboratory Animal Care guidelines and were allowed to acclimatize for at least 4 days prior to experiments. All animal experiments were performed in compliance with the institutional guidelines and approved by the Animal Use and Care Administrative Advisory Committee of West China Hospital, Sichuan University. BALB/c mice were randomly assigned into four groups ($n=4$), and they were injected intravenously (bolus injection) with PBS control, PDDA-QDs, CA-QDs, and PEG-QDs, respectively. The injection volume was 1% of body weight (eg, 230 µL QDs was injected into the mice with the body weight of 23 g), and the final injection dose of all QDs was 10 nmol/kg, which is approximately equivalent to 12.5 mg/kg. Twenty microliters of blood were collected from each mouse at 5, 15, 30, 60, 120, and 240 minutes postinjection, respectively. The blood was centrifuged at 2,000 rpm for 5 minutes, and QDs in the serum were detected by the fluorescence measurement using NanoDrop Fluorospectrometer (Thermo Fisher Scientific). Major organs, including heart, liver, spleen, kidney, and brain were harvested at 4 hours or 24 hours postinjection, respectively. Excised organs were frozen in optimal cutting temperature (cryo-embedding medium) at -80°C . The corresponding slices (10 µm) were then prepared with a cryostat, air-dried for 30 minutes, and fixed with 4% paraformaldehyde for 10 minutes. The nuclei were stained with 4',6-diamidino-2-phenylindole, and the slides were mounted with coverslips and visualized with a confocal fluorescence microscopy.

Statistical analysis

Statistical analysis was performed by Student's *t*-test for the comparison of two groups, and one-way analysis of variance for multiple groups, followed by Newman-Keuls test. A value of $P < 0.05$ was considered statistically significant.

Results

Characterization of QDs with various surface coatings

According to the information provided by the manufacturer, all three QDs with various surface coatings had the same emission wavelength at 580 nm, and their quantum yield was more than 50%. The zeta potential of PDDA-QDs, CA-QDs, and PEG-QDs were +50 mV, -50 mV, and -10 to 0 mV,

respectively. The morphology and particle size of QDs were evaluated under TEM. As shown in Figure S1, all three QDs were spherical, and homogeneous in size. The particle size of PDDA-QDs, CA-QDs, and PEG-QDs were all approximately 10 nm in diameter. No precipitation was observed when these QDs were incubated with different buffer, including Borate, Tris, and PBS (data not shown), suggesting their good colloidal stability in aqueous solution. To predict the in vivo stability of QDs after intravenous administration, the particle size distribution of QDs in the presence of FBS (50%) were measured by DLS and TEM, respectively. As shown in Figure S2, the particle size of CA-QDs and PEG-QDs in the presence of FBS were uniform and monodisperse, with the average size of approximately 8 nm. However, PDDA-QDs displayed two separate particle size populations in FBS and the average size in one population ranged from 1,000 to 10,000 nm, indicating that PDDA-QDs were not stable in FBS and tended to form large aggregates. Furthermore, this result was consistent with the observation under TEM (Figure S3).

Cellular uptake, pathways, and intracellular fates of QDs

QDs with different surface charges were incubated with MDA-MB-231 breast cancer cells in the serum-free medium at 37°C for different time points (30 minutes, 1, 2, and 4 hours). Initially, the internalization of QDs was visualized under a confocal fluorescence microscopy. As shown in Figure 1, QDs were

gradually taken up by MDA-MB-231 cells in a time-dependent manner. The red fluorescence coming from QDs was detected inside the cytosolic compartments of MDA-MB-231 cells, indicating that QDs were internalized in the cells. The fluorescence intensity indicated the level of the internalization of QDs by cells. The cellular uptake of QDs was not detectable at 30 minutes after the exposure, and gradually increased from 1 to 4 hours. In general, charged QDs (either positive or negative) were taken up dramatically higher than uncharged counterparts in MDA-MB-231 cells, and negatively charged QDs had higher uptake than positively charged ones.

The pathways involved in the uptake process of QDs were next explored. First of all, the cellular uptake of all QDs was an energy-dependent process (active transport), as evidenced by the significant decrease in the uptake of all QDs at low temperature (4°C) ($P < 0.05$). Then, three different endocytosis inhibitors, each known to be specific against a particular endocytic pathway, were employed to determine the cellular uptake mechanisms of the QDs. As shown in the confocal images (Figure 2A), all these endocytosis inhibitors were able to inhibit the cellular uptake of different charged QDs to varying extent, when compared to the corresponding controls without the prior treatment of endocytosis inhibitors. Among them, CPZ inhibited the cellular uptake of all QDs to the greatest extent, indicating that clathrin-mediated endocytosis was likely the dominant route. The inhibition efficiency of QDs uptake by these

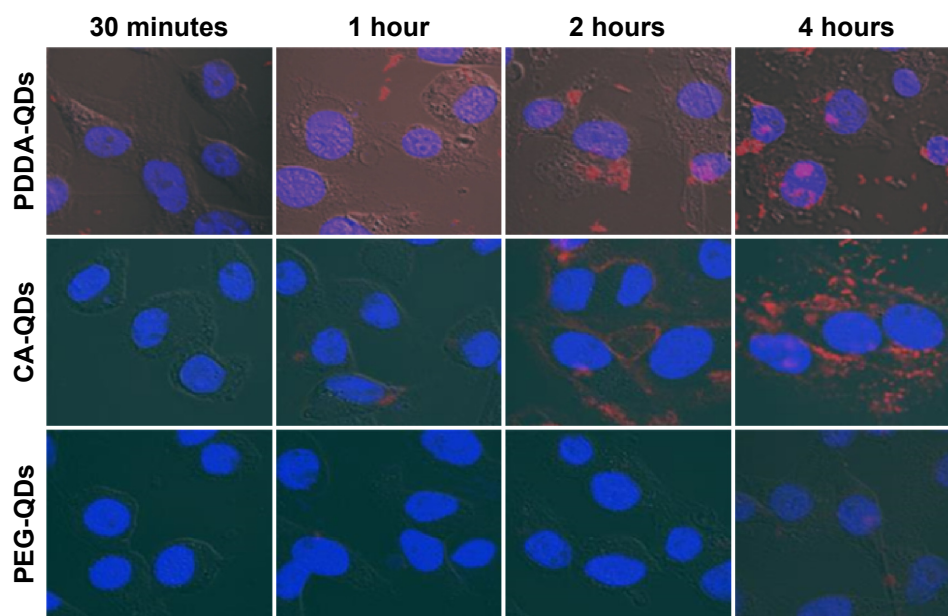


Figure 1 Cellular uptake of various QDs.

Notes: Confocal microscopic images showing the cellular uptake of PDDA-QDs, CA-QDs, and PEG-QDs in MDA-MB-231 cells after different incubation time. The nuclei were counterstained by Hoechst 33342. The red fluorescence intensity indicated the level of the internalization of QDs by cells.

Abbreviations: CA, carboxylic acid; PDDA, polydiallyldimethylammonium chloride; PEG, polyethylene glycol; QDs, quantum dots.

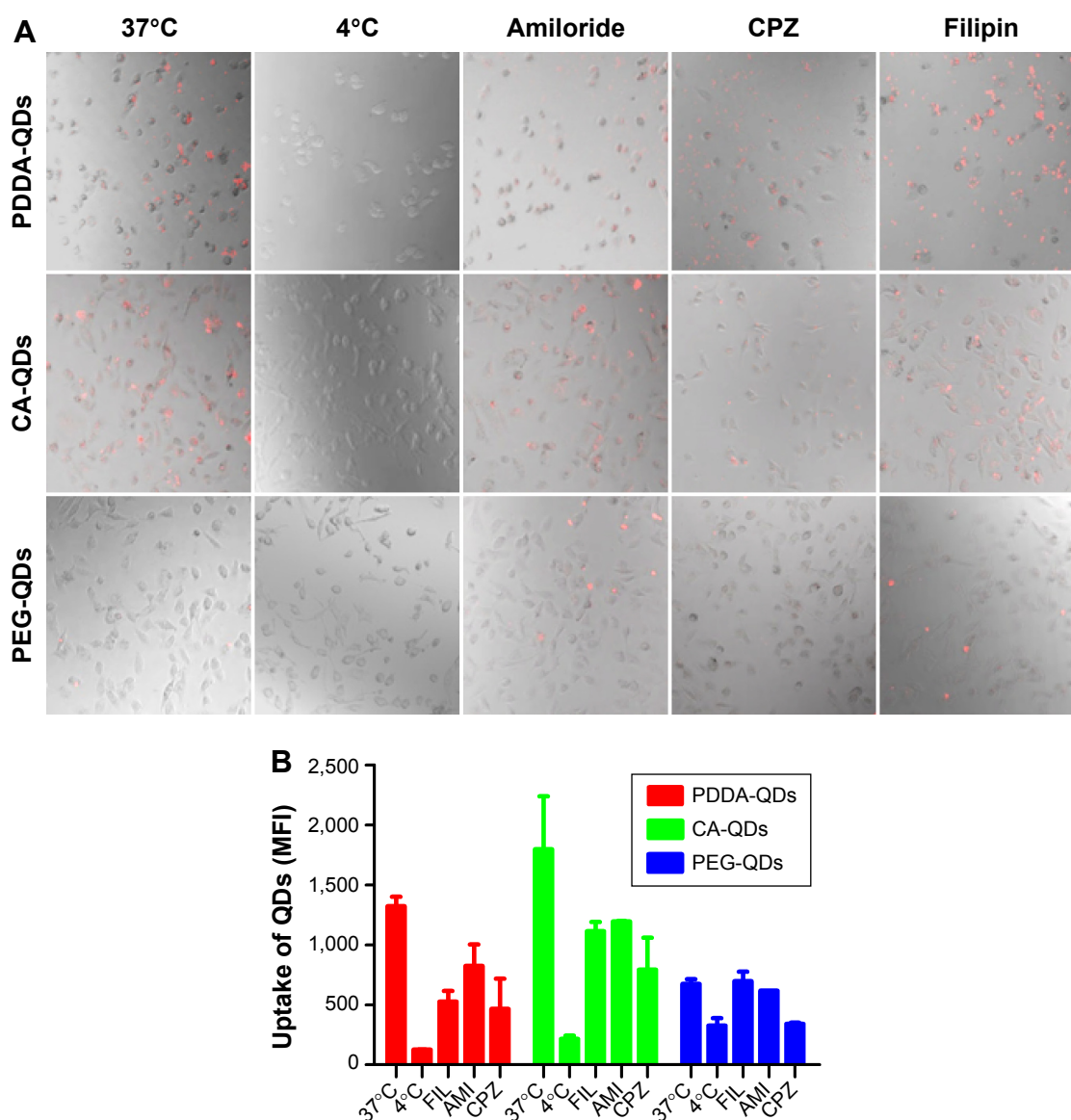


Figure 2 The uptake pathways of different charged QDs in MDA-MB-231 cells.

Notes: The effects of temperature and endocytosis inhibitors on the cellular uptake of QDs were analyzed by confocal fluorescence microscopy (A; 200 \times magnification) and flow cytometry (B), respectively. MDA-MB-231 Cells were either preincubated at 4°C for 1 hour, followed by incubation with different QDs at 4°C for 2 hours; or pretreated with different endocytosis inhibitors such as amiloride (50 mM), chlorpromazine (CPZ, 10 mg/mL) and filipin III (1 mg/mL) at 37°C for 1 hour, followed by incubation with different QDs at 37°C for 2 hours.

Abbreviations: AMI, amiloride; CA, carboxylic acid; FIL, filipin; PDDA, polydiallyldimethylammonium chloride; PEG, polyethylene glycol; QDs, quantum dots.

endocytosis inhibitors was further quantitatively analyzed by flow cytometry. As shown in Figure 2B, when MDA-MB-231 cells were preincubated with filipin III, the uptake of PDDA-QDs, CA-QDs, and PEG-QDs were reduced by approximately 34%, 28%, and -3%, respectively; Similarly, when cells were preincubated with amiloride, the uptake of PDDA-QDs, CA-QDs, and PEG-QDs were reduced by approximately 38%, 34%, and 8%, respectively. More remarkably, when cells were preincubated with CPZ, the uptake of PDDA-QDs, CA-QDs, and PEG-QDs were reduced by approximately 65%, 56%, and 40%, respectively. Taken together, several endocytic pathways

were involved in the uptake process of QDs, and clathrin-mediated endocytosis was the dominant one.

The intracellular fates of QDs upon their uptake were further investigated. First, co-localization studies^{21,28} were performed to track the subcellular localization of QDs. The lysosomes and mitochondria compartments of RAW 264.7 cells were stained with the LysoTracker Green probe and DiOC6(3), respectively. The co-localization of QDs (red) with lysosomes (green) or mitochondria (green) displays yellow fluorescence in the merged images. As shown in confocal images (Figure 3A), all QDs were partially localized in lysosomes but not in mitochondria. Then, the intracellular

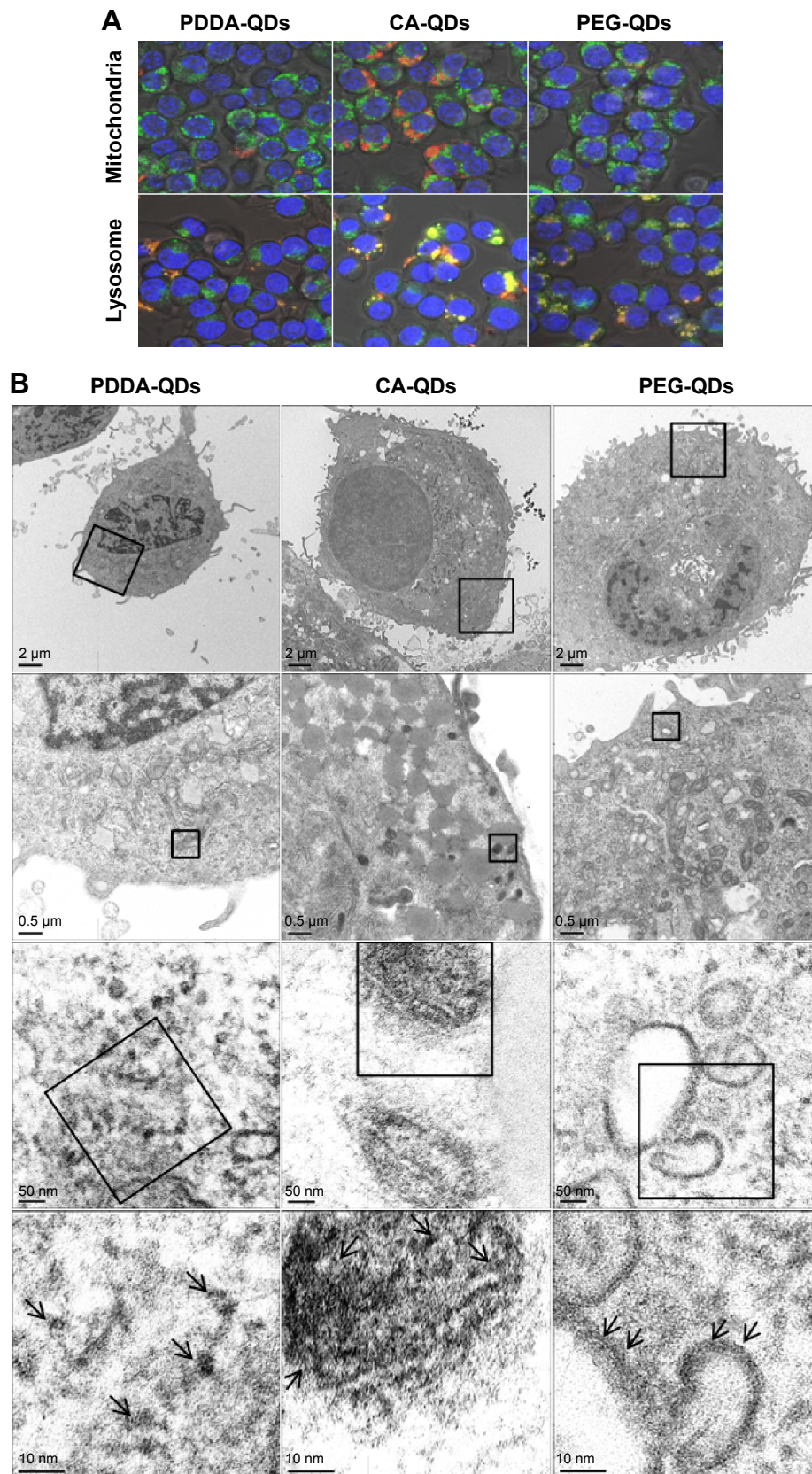


Figure 3 The intracellular distribution of QDs.

Notes: (A) Intracellular tracking of different charged QDs in RAW 264.7 macrophages. RAW 264.7 cells were incubated with different charged QDs for 2 hours, and then the cells were labeled with DiOC6(3) (green) or lysosome tracker (green) for 30 minutes before imaging by confocal microscopy. Co-localization of QDs with mitochondria or lysosome appears yellow in merged images, indicating that the QDs locate in the mitochondria or lysosome. 400× magnification. (B) TEM images of MDA-MB-231 cells exposed to different charged QDs. MDA-MB-231 cells were exposed to different QDs for 2 hours at 40 nM. The arrows show the location of QDs in the cells.

Abbreviations: CA, carboxylic acid; PDDA, polydiallyldimethylammonium chloride; PEG, polyethylene glycol; QDs, quantum dots; TEM, transmission electron microscope.

distribution of QDs was also visualized by TEM (Figure 3B). The fates of QDs in MB-MA231 cells were completely different depending on the surface charge. Pyknosis and karyorrhexis were the characters of cells incubated with PDDA-QDs, and PDDA-QDs mainly dispersed in the cytosol. At the same incubation time, CA-QDs could enter the cells more effectively compared with the other two types of QDs, and most CA-QDs tended to accumulate in endosome and lysosome. PEG-QDs were observed to localize in the cytoplasm and the periphery of vesicles (eg, endosomes, lysosomes, and lipid droplets).

Cytotoxicities and underlying mechanisms of QDs

The in vitro cytotoxicities of QDs with various surface charges were evaluated by MTS assay. As illustrated in Figure 4, no appreciable cytotoxicity against three different cell lines (RAW 264.7 macrophages, MDA-MB-231, and BT-20 breast cancer cells) were observed for CA-QDs and

PEG-QDs at the tested concentrations varying from 1.25 to 40 nM. However, concentration-dependent cytotoxicity was found in the case of PDDA-QDs ($P < 0.05$).

LDH assay was performed to monitor the cell membrane integrity after the treatment of QDs. LDH inside cells is released into the culture medium following the loss of membrane integrity resulting from either apoptosis or necrosis. As shown in Figure 5A, the treatment of positively charged PDDA-QDs in MDA-MB-231 cells led to the release of LDH in a dose-dependent manner, indicating that PDDA-QDs could disrupt the integrity of cell membranes. On the contrary, no LDH release was found in cells treated with both CA-QDs and PEG-QDs at concentrations up to 80 nM.

The hemolytic activities of QDs with various surface charges were evaluated using hemolysis assay. Different charged QDs were incubated with mouse erythrocytes suspension at 37°C for 4 hours, respectively. The results demonstrated that both CA-QDs and PEG-QDs had negligible hemolytic activities at the concentrations ranging from 2.5 to

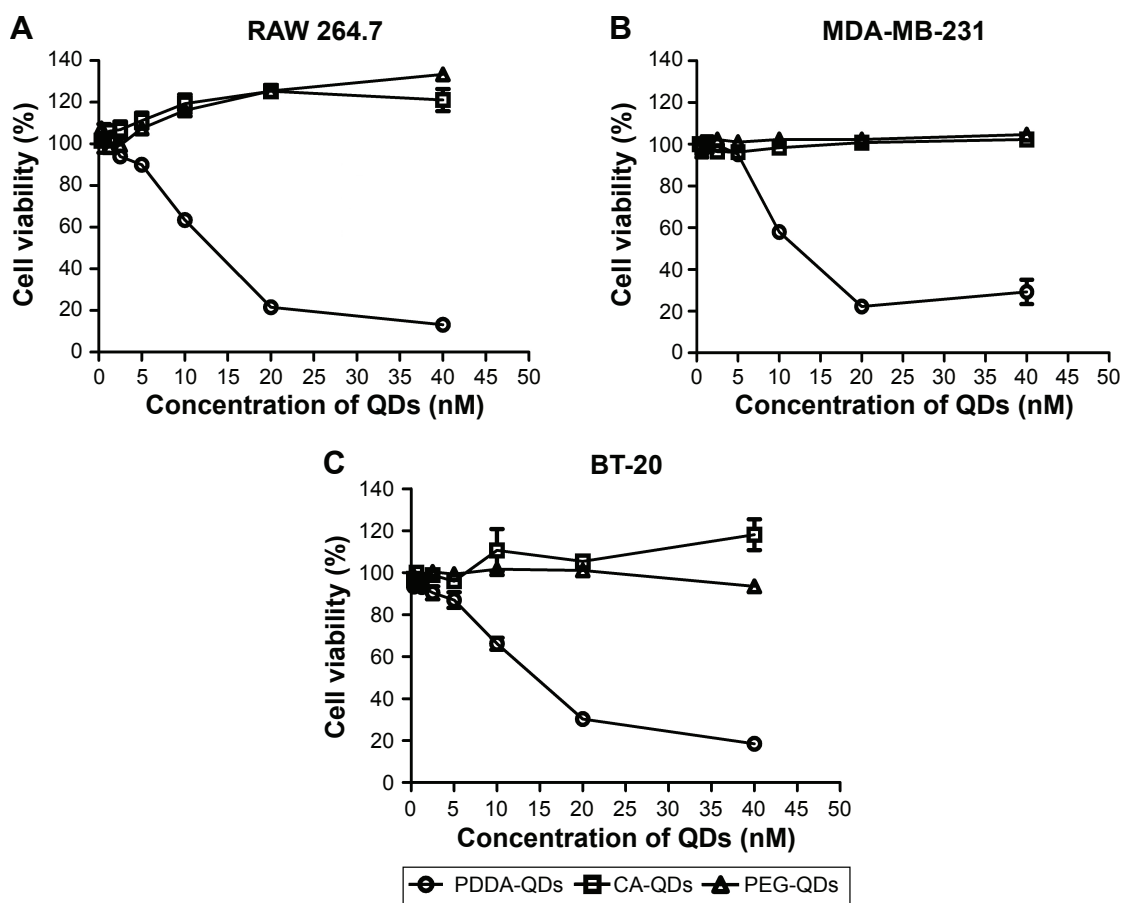


Figure 4 The in vitro cytotoxicities of different charged QDs against three cell lines.

Notes: RAW 264.7 macrophages (A), MDA-MB-231 breast cancer cells (B), and BT-20 breast cancer cells (C) were treated with different concentrations of QDs, respectively. After 24-hour incubation, the cell viability was measured by MTS assay.

Abbreviations: CA, carboxylic acid; PDDA, polydiallyldimethylammonium chloride; PEG, polyethylene glycol; QDs, quantum dots.

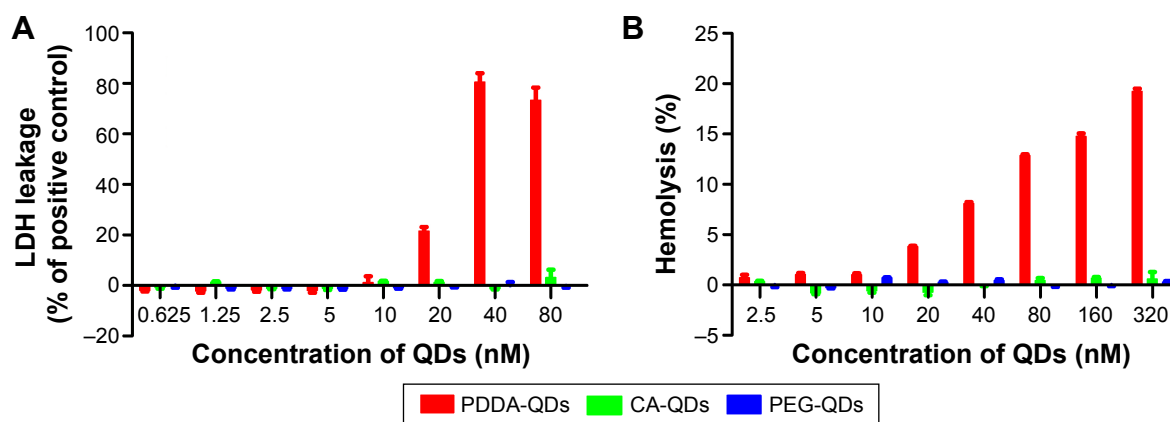


Figure 5 The LDH toxicity and hemolytic activity of different charged QDs.

Notes: (A) LDH release in MDA-MB-231 cells incubated with different charged QDs for 2 hours. (B) In vitro red blood cells (RBCs) lysis. Mouse erythrocyte suspension was incubated with different charged QDs for 4 hours at 37°C.

Abbreviations: CA, carboxylic acid; LDH, lactate dehydrogenase; PDDA, polydiallyldimethylammonium chloride; PEG, polyethylene glycol; QDs, quantum dots.

320 nM, whereas PDDA-QDs exhibited dose-dependent hemolytic properties (Figure 5B).

Dual staining with fluorescent Annexin V, and PI was used to discriminate apoptotic and necrotic cell death. We found that both CA-QDs and PEG-QDs did not induce either apoptosis or necrosis in MDA-MB-231 cells (data not shown), whereas PDDA-QDs induced both apoptosis and necrosis depending on the dose (Figure 6A). At higher concentrations, the necrotic effect of PDDA-QDs became more prominent, with a minimal number of apoptotic cells.

The production of intracellular ROS in cells after exposure to different charged QDs was measured by DCF-DA assay. As shown in confocal images (Figure 6B), negatively charged and neutral QDs did not induce obvious redox stress in MDA-MB-231 cells at concentrations up to 40 nM, when compared with negative control. In contrast, positively charged PDDA-QDs caused significant enhancement in intracellular ROS production at concentrations ranging from 10 to 40 nM. The dose-dependent enhancement of ROS production by PDDA-QDs was further quantitatively confirmed by flow cytometric analysis (Figure 6C).

Since oxidative stress is known to impair mitochondria, the effect of different charged QDs on mitochondrial membrane potential (MMP) in MDA-MB-231 cells was also investigated. Figure 6D demonstrated that only slight reduction of MMP were found for PEG-QDs and CA-QDs at the concentrations up to 40 nM, while obvious reduction of MMP was induced by PDDA-QDs in a dose-dependent manner.

All QDs, regardless of surface charges, did not affect the cell cycle after 24-hour exposure in MDA-MB-231 cells at concentrations up to 10 nM (Figure S4).

In vivo toxicity, blood clearance, and biodistribution studies of QDs

QDs with various surface charges at the dose of 10 nmol/kg (equivalent to 12.5 mg/kg) were injected intravenously into BALB/c mice, respectively. In mice treated with CA-QDs or PEG-QDs, no animal death occurred. However, for PDDA-QDs-treated mice, all the mice died within 24 hours postinjection. This result suggested that the surface coatings of QDs had a profound influence on their in vivo toxicity.

The blood clearance and tissue biodistribution profiles of all QDs in BALB/c mice were next investigated. Due to the intrinsic optical property of QDs, fluorescence detection provides a semiquantitative measurement of QDs behavior in vivo. The fluorescence intensity of QDs in the mouse serum was measured at different time points postinjection. The result in Figure 7A revealed that the surface charge had a dramatic influence on the blood clearance of QDs. Negatively charged and neutral QDs showed similar blood circulation profiles, and their circulation time was approximately 4 hours. In contrast, positively charged PDDA-QDs were almost undetectable in the blood immediately after the intravenous injection. The major organs, including the heart, liver, spleen, kidneys, and brain, were excised for ex vivo microscopic fluorescence imaging at 4 hours or 24 hours postinjection. Figure 7B illustrated the differential uptake of various QDs in different tissues at 4 hours. Compared with PBS control, CA-QDs and PEG-QDs had strong red fluorescence signal in the liver and the spleen, with almost no signal in heart, kidney, and brain. On the contrary, PDDA-QDs had a high uptake in the kidney, other than in the liver and spleen. Notably, PDDA-QDs, but not CA-QDs and PEG-QDs, were found to be present in the brain tissue, suggesting that

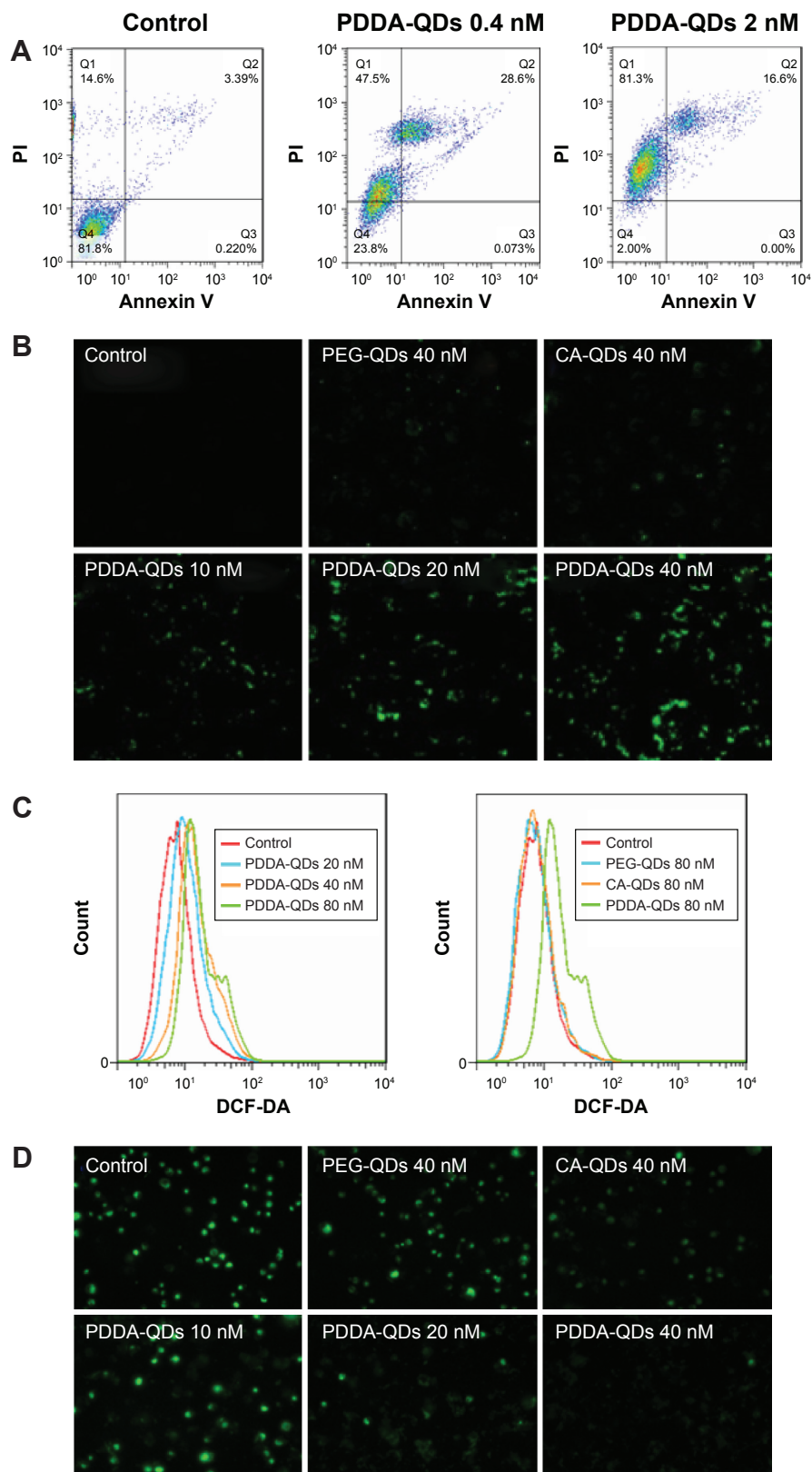


Figure 6 The underlying mechanisms of QDs cytotoxicity.

Notes: Apoptotic or necrotic cell death (A) of MDA-MB-231 cells was detected by flow cytometry after 24-hour incubation with PDDA-QDs, followed by Annexin V-FITC and PI dual-staining. Intracellular reactive oxygen species (ROS) production in MDA-MB-231 cells treated with different charged QDs was detected by confocal microscopy (B) and flow cytometry (C), respectively. Intracellular ROS was measured using 10 μ M DCF-DA probe. (D) The membrane mitochondria potential of MDA-MB-231 cells was acquired with fluorescence microscopy. Cells were incubated with various concentrations of QDs for 2 hours, and treated with 40 nM of DiOC6(3) for 30 minutes.

Abbreviations: CA, carboxylic acid; DCF-DA, 2',7'-Dichlorofluorescein diacetate; FITC, fluorescein isothiocyanate; PDDA, polydiallyldimethylammonium chloride; PI, propidium iodide; PEG, polyethylene glycol; QDs, quantum dots.

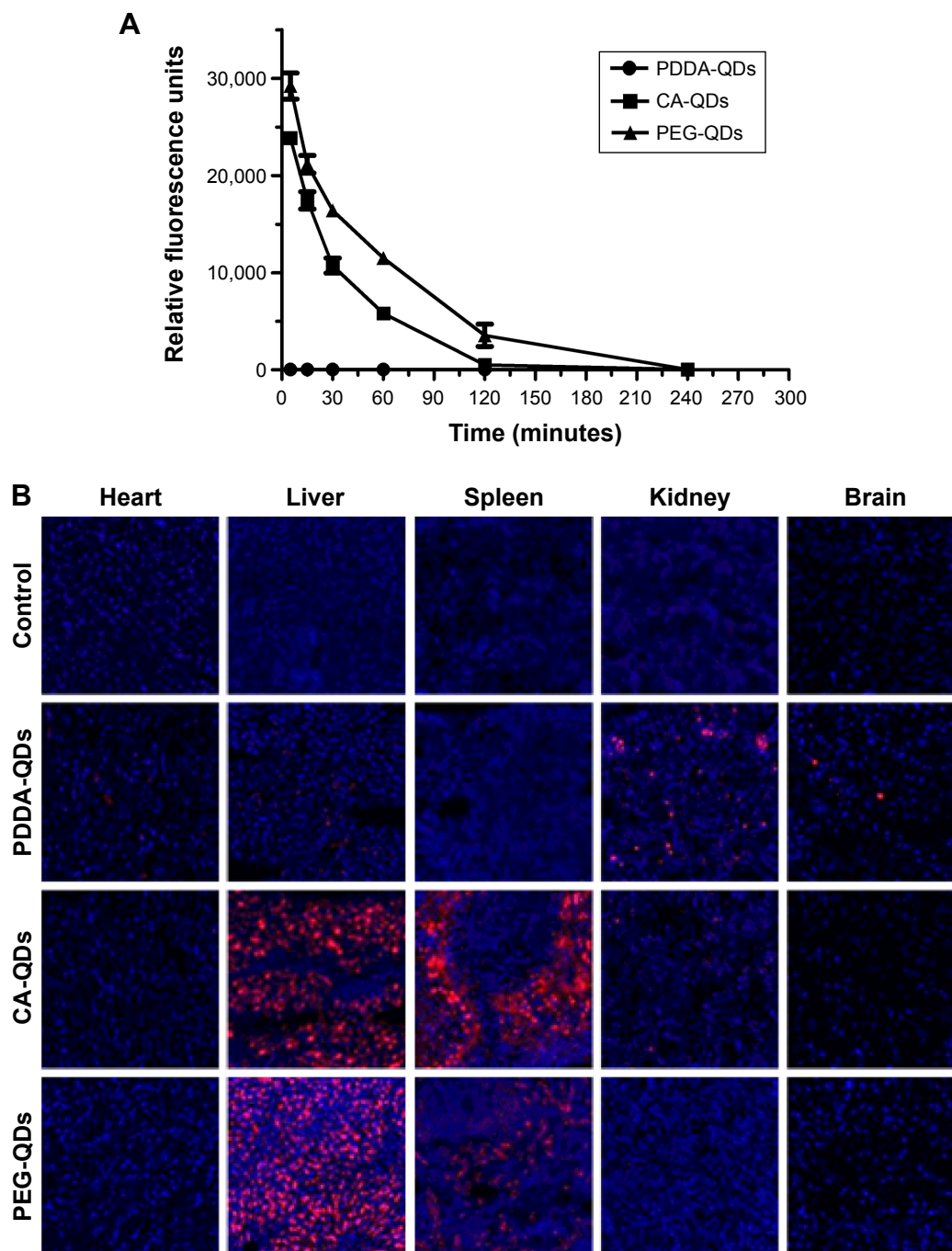


Figure 7 In vivo blood clearance and tissue biodistribution.

Notes: In vivo blood clearance (**A**) and tissue biodistribution (**B**) of different charged QDs in BALB/c mice after intravenous administration. QDs in the serum were detected by the fluorescence measurement using NanoDrop Fluorospectrometer. The major organs were excised for microscopic examination at 4 hours postinjection. The organ slices (10 μ m) were prepared with a cryostat, air-dried for 30 minutes, and fixed with 4% paraformaldehyde for 10 minutes. The nuclei were stained by DAPI (blue), and the signal of QDs (red) was acquired with confocal fluorescence microscopy. Magnification \times 200.

Abbreviations: CA, carboxylic acid; DAPI, 4',6-diamidino-2-phenylindole; PDDA, polydiallyldimethylammonium chloride; PEG, polyethylene glycol; QDs, quantum dots.

PDDA-QDs may be able to cross the blood–brain barrier. At 24 hours postinjection, the signal of PEG-QDs in the liver and the spleen was almost undetectable, but that of CA-QDs in both the liver and the spleen remained high (Figure S5), indicating that CA-QDs have a much slower elimination rate than PEG-QDs.

Discussion

As the achievements of QDs in biomedical field are inspiring pharmaceutical researchers to develop them as novel nanomedicines for clinical use, we need to evaluate the biological effects of QDs more carefully and comprehensively. To date, only limited studies have been performed to explore

the effects of surface charge and chemistry on the biological behaviors of QDs, while many studies report that the surface charge plays a pivotal role in other nanoparticles.^{25,29} Our present study aimed to investigate the biological effects of various charged QDs and their underlying mechanisms. However, comparison of the uptake of QDs and toxicity could be confounded because of the diversity of QDs being synthesized. Not all QDs are alike and different QDs have their own properties, such as size, shape, composition, surface charge, and surface functionalization. In order to focus on the effect of surface charge, we tried to minimize the potential confounding factors by using commercially available QDs with different surface coatings (PDDA, CA, and PEG), but with the same composition (CdSe core/ZnS shell), particle size, and emission wavelength.

The impact of surface charge on cellular uptake of QDs has been studied sporadically, and the results have been so far controversial. Some groups reported preferential uptake of negatively charged QDs, while others reported high uptake of positively charged QDs.^{30,31} Our results demonstrated that all QDs with various surface charges were able to be taken up by MDA-MB-231 cells in a time-dependent manner. However, charged QDs had significantly higher cellular uptake than neutral ones, and the negatively charged QDs had the highest uptake among all these QDs. The preferential cellular uptake of charged nanoparticles other than neutral ones not only was found in our QDs study, but also in other nanoparticles, such as albumin particles, and polymeric nanoparticles.^{25,32} The reason why negatively charged particles have the highest uptake is unknown. This is probably due to the higher hydrophobicity of negative particles compared to the corresponding neutral and positive ones.³³

The mechanisms of QDs cellular entry may be different depending on the surface charge. The blockage of QDs uptake in MDA-MB-231 cells at low temperature suggested that all the QDs entered the cells via active transport. It was previously reported that endocytosis is the major entry route for most nanoparticles including QDs.³⁴ In our study, three different endocytosis inhibitors, including filipin III (caveolae-mediated endocytosis inhibitor), amiloride (macropinocytosis inhibitor), and CPZ (clathrin-mediated endocytosis inhibitor), were employed to explore the uptake pathways of these QDs. We found that clathrin-mediated endocytosis was the dominant entry route for all QDs independent of surface charge, although caveolae-mediated endocytosis and macropinocytosis were partially involved in their uptake process. Consistent with our observation in QDs, several other types of nanoparticles, such as FITC-labeled SPION

and PEG-poly(lactic acid), have also been shown to enter cells through clathrin-mediated endocytosis.^{35,36}

The intracellular localization of QDs with various surface charges was illustrated by both confocal images and TEM observation. QDs were localized in different subcellular compartments (eg, cytoplasm and vesicles) depending on their surface charge. This observation was consistent with previous reports. For example, Xiao et al reported that negatively charged QD655-COOH co-localized with lysosomes upon the cellular uptake in MCF-7 cells.³⁷ Lovrić et al observed that 5.2 nm cationic CdTe QDs localized throughout the cytoplasm of N9 cells.²¹ Ryman-Rasmussen et al reported that PEG-coated QD 565 dispersed in cytoplasm and the periphery of lipid droplets.³⁸

One major obstacle to clinical applications of QDs is the concern over their possible cytotoxicity. Surface charge, including charge density and charge polarity, plays a critical role in the cytotoxic action of QDs. We demonstrated that positively charged QDs exhibited much higher cytotoxicity than negatively charged and neutral counterparts in both phagocytic and nonphagocytic cells. Previous studies also reported that positively charged zinc, gold, and silica nanoparticles are more cytotoxic than negative variants of similar size in nonphagocytic and phagocytic cells.³⁹⁻⁴¹ The cytotoxicity of positively charged PDDA-QDs was not determined by the intracellular uptake. Indeed, the cellular uptake of PDDA-QDs was lower than that of CA-QDs; however, the cytotoxicity of PDDA-QDs was dramatically higher than that of CA-QDs. Clearly, the disastrous cytotoxicity of PDDA-QDs was dominated by the positive surface coating. It has been demonstrated that cationic polymers such as polyethylenimine and poly(L-lysine) may exert their cytotoxicity by inducing necrosis or apoptosis through mitochondria-mediated pathways.⁴² The potential mechanisms underlying the cytotoxicity of PDDA-QDs were explored in our study. First, PDDA-QDs induced both apoptosis and necrosis, and necrosis dominated at the high dose. Second, PDDA-QDs were able to disrupt the integrity of the cell membrane, which was evidenced by LDH leakage, and hemolytic activity in the cells treated with PDDA-QDs. Third, PDDA-QDs dramatically increased the production of ROS, which will result in serious damage to cell structures, and induce cell death through apoptosis and necrosis. Finally, PDDA-QDs induced the dose-dependent mitochondrial stress (the reduction of MMP) in cells. Mitochondria are organelles that are very sensitive to QDs-induced stress.⁴³

The effect of surface charge on *in vivo* toxicity, pharmacokinetics, tissue distribution and elimination of QDs has

rarely been interrogated. Herein, we demonstrated that surface coatings had tremendous impact on the biological effects and in vivo fates of QDs. No animal death was found in mice treated with negatively charged and neutral QDs; however, all the mice treated with positively charged QDs were dead within 24 hours postinjection. The reasons responsible for the animal death occurred in the PDDA-QDs group are unknown. Although PDDA has been widely used to construct or decorate different nanoparticles for drug delivery and therapeutic purposes, the toxicities of PDDA with different cores have not been studied.^{44,45} We suspected that PDDA-QDs-induced animal death was probably attributed to the rapid hemolysis, or the formation of large aggregates, which may occlude the capillary. Tang et al demonstrated that positive QDs displayed severe acute toxicity, and they attributed the toxicity to the coating material PDDA.⁴⁶ Suresh et al also demonstrated the PDDA-coated Ag nanoparticles were more toxic than other coating nanoparticles, such as biogenic-Ag, oleate-Ag nanoparticles.⁴⁷ The blood clearance profile of QDs was dramatically affected by the surface charge. The blood circulation time of negatively charged and neutral QDs was 2–4 hours, whereas positively charged QDs were almost undetectable in the blood immediately after the injection. It is possible that positively charged QDs interact with blood cell membranes, serum proteins, form large aggregates, and the large aggregates would be spun down to the bottom of the vials with blood cells when we measured the fluorescence of serum. Furthermore, previous reports have also indicated that positively charged nanoparticles are cleared out from circulation within minutes.⁴⁸ The tissue distribution and elimination of QDs were also strongly depending on their surface charges. Negatively charged and neutral QDs were mainly trapped in the liver and the spleen, which were ascribed to the clearance of nanoparticles from the blood by cells of the mononuclear phagocyte system.⁴⁹ In contrast, positively charged QDs had low uptake in both liver and spleen, but with relatively high uptake in the kidney. More importantly, it was unexpected that positively charged QDs were also present in the brain tissue, suggesting they are able to cross the blood–brain barrier. To the best of our knowledge, this is the first case to report that positive charge may facilitate the entry of QDs in the brain. The specific mechanism underlying this phenomenon is unknown yet. It might be ascribed to the opening the tight junctions around the capillaries by positively charged QDs.⁵⁰ As shown in our study, the tissue-specific distribution of QDs could be readily controlled by modulating their surface charges, and this information will be very useful for the targeted imaging and drug delivery of QDs.

Conclusion

In summary, surface charge had a huge impact on the biological effects of QDs. We demonstrated that charged QDs were taken up higher than neutral counterparts in MDA-MB-231 cells, and negatively charged QDs exhibited the highest uptake among all QDs. All QDs were actively taken up by an endocytic process, and primarily through clathrin-mediated endocytosis. Interestingly, the subcellular localization of QDs upon the internalization was dependent of surface charge. Compared with negatively charged and neutral QDs, positively charged QDs exhibited dose-dependent cytotoxicity, which was probably because they disrupted the cell membrane integrity, induced intracellular ROS and mitochondrial stress. Negatively charged and neutral QDs had much longer blood circulation time than positively charged ones, and they preferentially accumulated in the liver and the spleen. In contrast, positively charged QDs are mainly distributed in kidney, with obvious uptake in the brain. Taken together, our results suggest that the surface charge plays important roles in modulating the biological responses of QDs in view of their biomedical applications.

Acknowledgments

This work was supported by the National Natural Sciences Foundation of China (numbers 81101143 and 81572617), the Sichuan University Outstanding Young Scholars Research Grant (2082604174150), and the Basic Research Foundation from the Science and Technology Bureau of Sichuan Province (2015JY0197).

Disclosure

The authors report no conflicts of interest in this work.

References

1. Michalet X, Pinaud FF, Bentolila LA, et al. Quantum dots for live cells, in vivo imaging, and diagnostics. *Science*. 2005;307(5709):538–544.
2. Dubertret B, Skourides P, Norris DJ, et al. In vivo imaging of quantum dots encapsulated in phospholipid micelles. *Science*. 2002;298(5599):1759–1762.
3. Medintz IL, Uyeda HT, Goldman ER, et al. Quantum dot bioconjugates for imaging, labelling and sensing. *Nat Mater*. 2005;4(6):435–446.
4. Tiwari DK, Jin T, Behari J. Bio-distribution and toxicity assessment of intravenously injected anti-HER2 antibody conjugated CdSe/ZnS quantum dots in Wistar rats. *Int J Nanomedicine*. 2011;6:463.
5. Gao X, Cui Y, Levenson RM, et al. In vivo cancer targeting and imaging with semiconductor quantum dots. *Nat Biotechnol*. 2004;22(8):969–976.
6. Madani SY, Shabani F, Dwek MV, et al. Conjugation of quantum dots on carbon nanotubes for medical diagnosis and treatment. *Int J Nanomedicine*. 2013;8:941.
7. Howarth M, Liu W, Puthenveetil S, et al. Monovalent, reduced-size quantum dots for imaging receptors on living cells. *Nat Methods*. 2008;5(5):397–399.

8. Åkerman ME, Chan WC, Laakkonen P, et al. Nanocrystal targeting in vivo. *Proc Natl Acad Sci U S A*. 2002;99(20):12617–12621.
9. Farlow J, Seo D, Broaders KE, et al. Formation of targeted monovalent quantum dots by steric exclusion. *Nat Methods*. 2013;10(12):1203–1205.
10. Dwarakanath S, Bruno JG, Shastry A, et al. Quantum dot-antibody and aptamer conjugates shift fluorescence upon binding bacteria. *Biochem Biophys Res Commun*. 2004;325(3):739–743.
11. Setyawati M, Tay CY, Chia S, et al. Titanium dioxide nanomaterials cause endothelial cell leakiness by disrupting the homophilic interaction of VE-cadherin. *Nat Commun*. 2013;4:1673.
12. Zhang X-Q, Xu X, Bertrand N, Pridgen E, Swami A, Farokhzad OC. Interactions of nanomaterials and biological systems: Implications to personalized nanomedicine. *Adv Drug Deliv Rev*. 2012;64(13):1363–1384.
13. Hoshino A, Fujioka K, Oku T, et al. Physicochemical properties and cellular toxicity of nanocrystal quantum dots depend on their surface modification. *Nano Lett*. 2004;4(11):2163–2169.
14. Jaiswal JK, Goldman ER, Mattoussi H, et al. Use of quantum dots for live cell imaging. *Nat Methods*. 2004;1(1):73–78.
15. Jaiswal JK, Mattoussi H, Mauro JM, et al. Long-term multiple color imaging of live cells using quantum dot bioconjugates. *Nat Biotechnol*. 2003;21(1):47–51.
16. Valizadeh A, Mikaeili H, Samiei M, et al. Quantum dots: synthesis, bioapplications, and toxicity. *Nanoscale Res Lett*. 2012;7(1):1–14.
17. Hardman R. A toxicologic review of quantum dots: toxicity depends on physicochemical and environmental factors. *Environ Health Perspect*. 2006;116:165–172.
18. Park MV, Neigh AM, Vermeulen JP, et al. The effect of particle size on the cytotoxicity, inflammation, developmental toxicity and genotoxicity of silver nanoparticles. *Biomaterials*. 2011;32(36):9810–9817.
19. Huang X, Teng X, Chen D, Tang F, He J. The effect of the shape of mesoporous silica nanoparticles on cellular uptake and cell function. *Biomaterials*. 2010;31(3):438–448.
20. Jiang J, Oberdörster G, Biswas P. Characterization of size, surface charge, and agglomeration state of nanoparticle dispersions for toxicological studies. *J Nanopart Res*. 2009;11(1):77–89.
21. Lovrić J, Bazzi HS, Cuie Y, Fortin GR, Winnik FM, Maysinger D. Differences in subcellular distribution and toxicity of green and red emitting CdTe quantum dots. *J Mol Med*. 2005;83(5):377–385.
22. Alexis F, Pridgen E, Molnar LK, Farokhzad OC. Factors affecting the clearance and biodistribution of polymeric nanoparticles. *Mol Pharm*. 2008;5(4):505–515.
23. Roberts JR, Antonini JM, Porter DW, et al. Lung toxicity and biodistribution of Cd/Se-ZnS quantum dots with different surface functional groups after pulmonary exposure in rats. *Part Fibre Toxicol*. 2013;10(5):1–17.
24. Juliano R, Stamp D. The effect of particle size and charge on the clearance rates of liposomes and liposome encapsulated drugs. *Biochem Biophys Res Commun*. 1975;63(3):651–658.
25. Xiao K, Li Y, Luo J, et al. The effect of surface charge on in vivo biodistribution of PEG-oligocholeic acid based micellar nanoparticles. *Biomaterials*. 2011;32(13):3435–3446.
26. Fröhlich E. The role of surface charge in cellular uptake and cytotoxicity of medical nanoparticles. *Int J Nanomed*. 2012;7:5577.
27. Manshian BB, Soenen SJ, Al-Ali A, et al. Cell type-dependent changes in cdse/ZnS quantum dot uptake and toxic endpoints. *Toxicol Sci*. 2015;144(2):246–258.
28. Clift MJ, Brandenberger C, Rothen-Rutishauser B, Brown DM, Stone V. The uptake and intracellular fate of a series of different surface coated quantum dots in vitro. *Toxicology*. 2011;286(1–3):58–68.
29. Schaeublin NM, Braydich-Stolle LK, Schrand AM, et al. Surface charge of gold nanoparticles mediates mechanism of toxicity. *Nanoscale*. 2011;3(2):410–420.
30. Sakai N, Matsui Y, Nakayama A, Tsuda A, Yoneda M. Functional-dependent and size-dependent uptake of nanoparticles in PC12. *J Phys Conf Ser*. 2011;304(1):012049.
31. Duan H, Nie S. Cell-penetrating quantum dots based on multivalent and endosome-disrupting surface coatings. *J Am Chem Soc*. 2007;129(11):3333–3338.
32. Roser M, Fischer D, Kissel T. Surface-modified biodegradable albumin nano-and microspheres. II: effect of surface charges on in vitro phagocytosis and biodistribution in rats. *Eur J Pharm Biopharm*. 1998;46(3):255–263.
33. Bu Q, Yan G, Deng P, et al. NMR-based metabolomic study of the sub-acute toxicity of titanium dioxide nanoparticles in rats after oral administration. *Nanotechnology*. 2010;21(12):125105.
34. Maysinger D, Lovrić J, Eisenberg A, Savić R. Fate of micelles and quantum dots in cells. *Eur J Pharm Biopharm*. 2007;65(3):270–281.
35. Harush-Frenkel O, Rozentur E, Benita S, Altschuler Y. Surface charge of nanoparticles determines their endocytic and transcytotic pathway in polarized MDCK cells. *Biomacromolecules*. 2008;9(2):435–443.
36. Lu C-W, Hung Y, Hsiao J-K, et al. Bifunctional magnetic silica nanoparticles for highly efficient human stem cell labeling. *Nano Lett*. 2007;7(1):149–154.
37. Xiao Y, Forry SP, Gao X, Holbrook RD, Telford WG, Tona A. Research dynamics and mechanisms of quantum dot nanoparticle cellular uptake. *J Nanobiotechnol*. 2010;8–13.
38. Ryman-Rasmussen JP, Riviere JE, Monteiro-Riviere NA. Surface coatings determine cytotoxicity and irritation potential of quantum dot nanoparticles in epidermal keratinocytes. *J Invest Dermatol*. 2007;127(1):143–153.
39. Baek M, Kim I-S, Yu J, Chung HE, Choy JH, Choi SJ. Effect of different forms of anionic nanoclays on cytotoxicity. *J Nanosci Nanotechnol*. 2011;11(2):1803–1806.
40. Goodman CM, McCusker CD, Yilmaz T, Rotello VM. Toxicity of gold nanoparticles functionalized with cationic and anionic side chains. *Bioconjugate Chem*. 2004;15(4):897–900.
41. Bhattacharjee S, de Haan LH, Evers NM, et al. Role of surface charge and oxidative stress in cytotoxicity of organic monolayer-coated silicon nanoparticles towards macrophage NR8383 cells. *Part Fibre Toxicol*. 2010;7(1):25.
42. Hunter AC, Moghimi SM. Cationic carriers of genetic material and cell death: a mitochondrial tale. *Biochim Biophys Acta*. 2010;1797(6):1203–1209.
43. Li J, Zhang Y, Xiao Q, et al. Mitochondria as target of quantum dots toxicity. *J Hazard Mater*. 2011;194:440–444.
44. Kvitek L, Panáček A, Soukupova J, et al. Effect of surfactants and polymers on stability and antibacterial activity of silver nanoparticles (NPs). *J Phys Chem C*. 2008;112(15):5825–5834.
45. Fischer D, Dautzenberg H, Kunath K, et al. Poly(diallyldimethylammonium chlorides) and their N-methyl-N-vinylacetamide copolymer-based DNA-polyplexes: role of molecular weight and charge density in complex formation, stability, and in vitro activity. *Int J Pharm*. 2004;280(1–2):253–269.
46. Tang Y, Han S, Liu H, et al. The role of surface chemistry in determining in vivo biodistribution and toxicity of CdSe/ZnS core-shell quantum dots. *Biomaterials*. 2013;34(34):8741–8755.
47. Suresh AK, Pelletier DA, Wang W, Morrell-Falvey JL, Gu B, Doktycz MJ. Cytotoxicity induced by engineered silver nanocrystallites is dependent on surface coatings and cell types. *Langmuir*. 2012;28(5):2727–2735.
48. Owens DE, Peppas NA. Opsonization, biodistribution, and pharmacokinetics of polymeric nanoparticles. *Int J Pharm*. 2006;307(1):93–102.
49. Chavanpatil MD, Khadair A, Panyam J. Nanoparticles for cellular drug delivery: mechanisms and factors influencing delivery. *J Nanosci Nanotechnol*. 2006;6(9–10):2651–2663.
50. Lockman PR, Koziara JM, Mumper RJ, Allen DD. Nanoparticle surface charges alter blood-brain barrier integrity and permeability. *J Drug Target*. 2004;12(9–10):635–641.

Supplementary materials

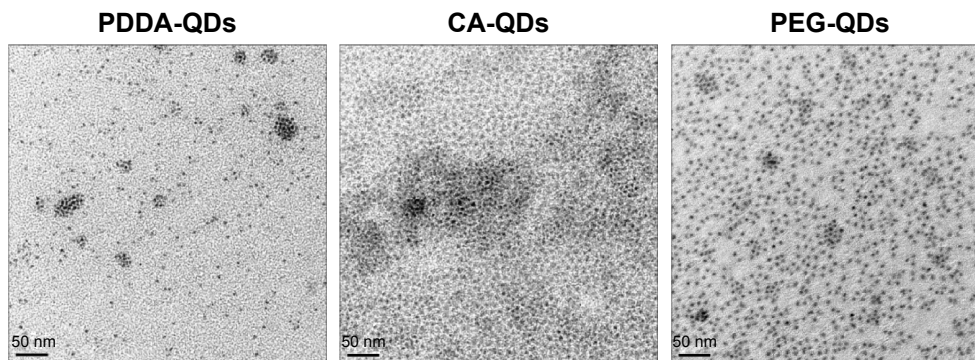


Figure S1 TEM images of QDs with various surface charges.

Note: The particle size of PDDA-QDs, CA-QDs, and PEG-QDs were all approximately 10 nm in diameter.

Abbreviations: CA, carboxylic acid; PDDA, polydiallyldimethylammonium chloride; PEG, polyethylene glycol; QDs, quantum dots; TEM, transmission electron microscope.

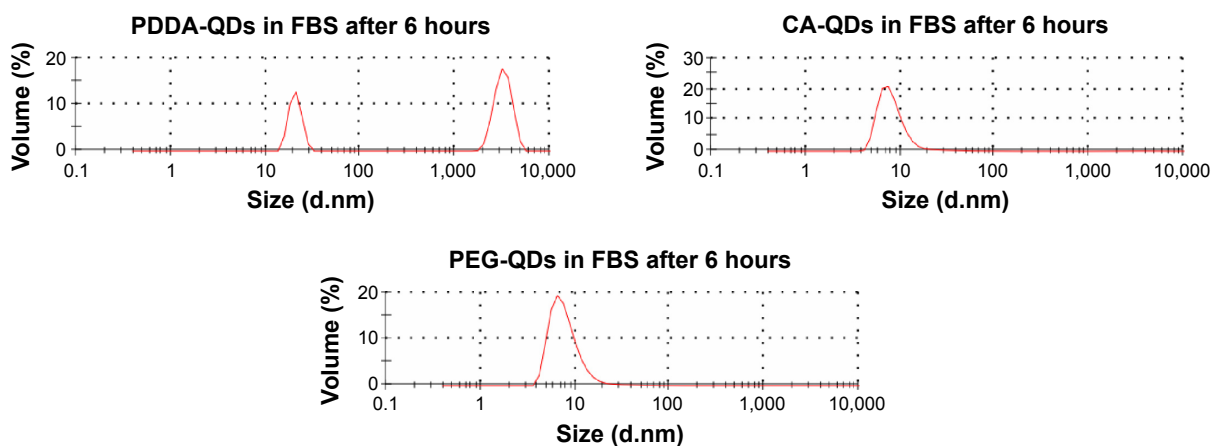


Figure S2 The stability of various QDs in fetal bovine serum (FBS, 50%) was monitored by the DLS size distribution measurement.

Note: In the presence of FBS, PDDA-QDs tended to form large aggregates, with the average size ranging from 1,000 to 10,000 nm.

Abbreviations: CA, carboxylic acid; DLS, dynamic light scattering; PDDA, polydiallyldimethylammonium chloride; PEG, polyethylene glycol; QDs, quantum dots.

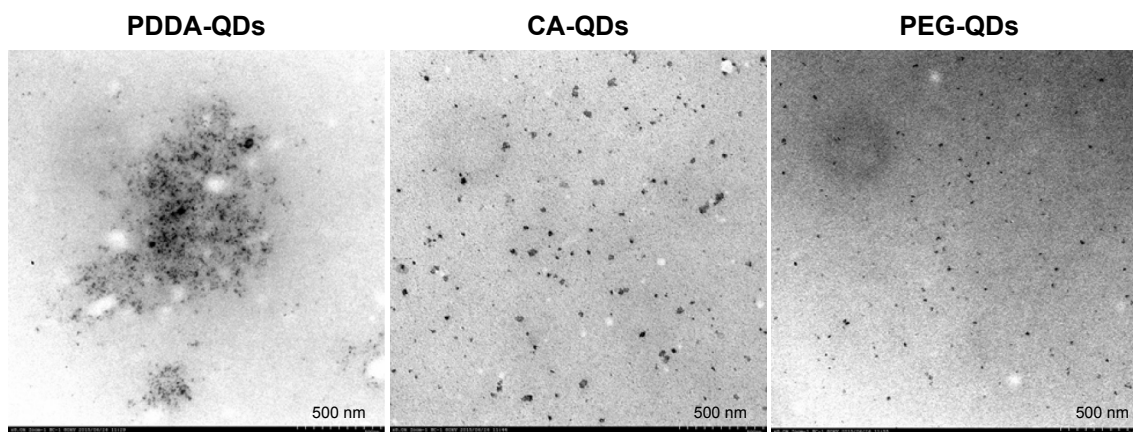


Figure S3 The stability of various QDs in FBS measured by TEM observation.

Note: After 6-hour incubation with FBS (50%), large aggregates were observed for PDDA-QDs, but not obvious for CA-QDs and PEG-QDs.

Abbreviations: CA, carboxylic acid; FBS, fetal bovine serum; PDDA, polydiallyldimethylammonium chloride; PEG, polyethylene glycol; QDs, quantum dots; TEM, transmission electron microscope.

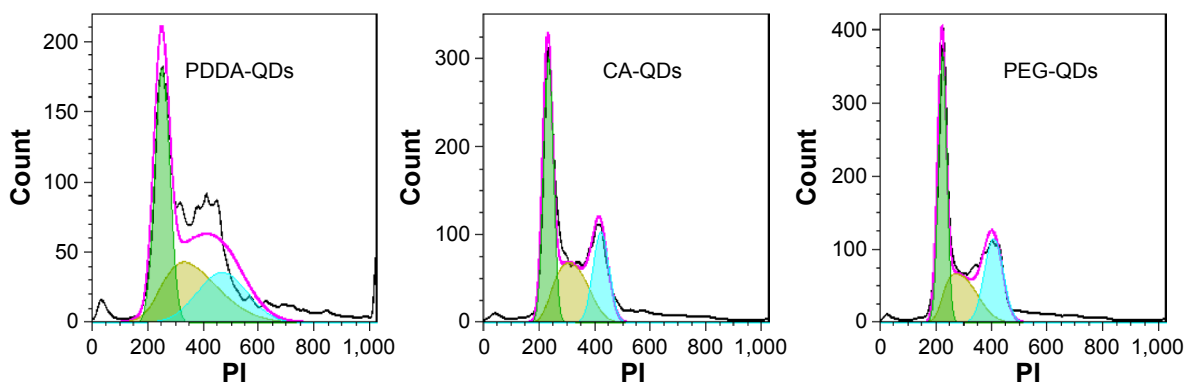


Figure S4 The cell cycle analysis of MDA-MB-231 cells treated with different charged QDs for 24 hours.

Abbreviations: CA, carboxylic acid; PDDA, polydiallyldimethylammonium chloride; PEG, polyethylene glycol; PI, propidium iodide; QDs, quantum dots.

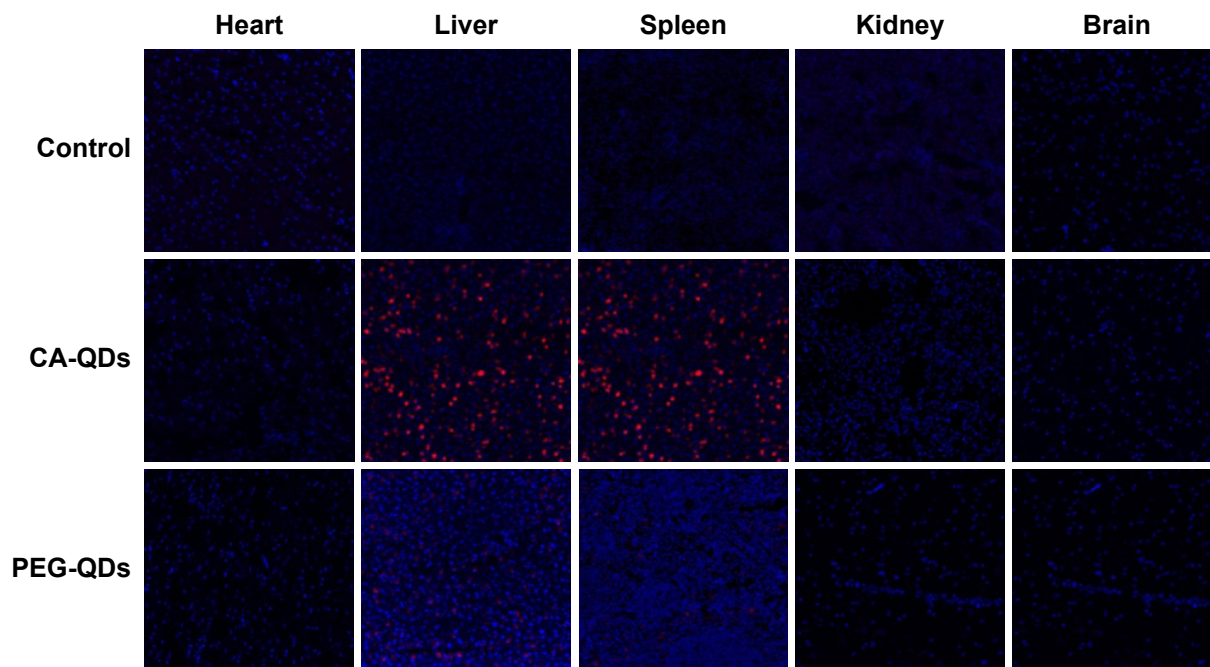


Figure S5 The tissue biodistribution of different charged QDs in major organs at 24 hours postinjection.

Note: The nuclei were stained by DAPI (blue), and the signal of QDs (red) was acquired with confocal fluorescence microscopy.

Abbreviations: CA, carboxylic acid; DAPI, 4',6-diamidino-2-phenylindole; PEG, polyethylene glycol; QDs, quantum dots.

International Journal of Nanomedicine

Dovepress

Publish your work in this journal

The International Journal of Nanomedicine is an international, peer-reviewed journal focusing on the application of nanotechnology in diagnostics, therapeutics, and drug delivery systems throughout the biomedical field. This journal is indexed on PubMed Central, MedLine, CAS, SciSearch®, Current Contents®/Clinical Medicine,

Journal Citation Reports/Science Edition, EMBase, Scopus and the Elsevier Bibliographic databases. The manuscript management system is completely online and includes a very quick and fair peer-review system, which is all easy to use. Visit <http://www.dovepress.com/testimonials.php> to read real quotes from published authors.

Submit your manuscript here: <http://www.dovepress.com/international-journal-of-nanomedicine-journal>